Fast Pyrolysis of Sisal Residue in a Pilot Fluidized Bed Reactor

Jambeiro, Taiane A.; Silva, Myller Fernandes S.; Pereira, Luis Gabriel G.; Vasconcelos, David da Silva; Silva, Gabriele Batalha; Figueiredo, Monique Bernardes; Lima, Sirlene Barbosa; Pires, Carlos Augusto M.

Published in:
Energy & fuels

DOI:
10.1021/acs.energyfuels.8b01718

Publication date:
2018

energy&fuels

Article

Cite This: Energy Fuels 2018, 32, 9478−9492

pubs.acs.org/EF

Fast Pyrolysis of Sisal Residue in a Pilot Fluidized Bed Reactor

Taiane A. Jambeiro,[†] Myller Fernandes S. Silva,[†] Luis Gabriel G. Pereira,[†] David da Silva Vasconcelos,[†] Gabriele Batalha Silva,[†] Monique Bernardes Figueirêdo,[‡] Sirlene Barbosa Lima,[†] and Carlos Augusto M. Pires*[,†]

[†]Chemical Reaction Engineering Laboratory, Federal University of Bahia, 40.210-910, Salvador, Bahia, Brazil

[‡]Department of Chemical Engineering, University of Groningen, Nijenborgh 4, 9747 AG Groningen, The Netherlands

ABSTRACT: The objective of this research was to study the fast pyrolysis of sisal residue, performed in a pilot unit with a fluidized bed reactor. The tests were carried out by varying the flows of nitrogen (8−14 N m^3/h), biomass (10.33−25.95 g/min), and temperature (450−550 °C). The experimental planning technique was used to identify the number of tests and the influence of operational variables on the bio-oil yield. One of the highest H_2/CO (2.16) ratios was found from the eighth test on, which was an appropriate value for the production of methanol and liquid biofuels. All bio-oil samples produced were characterized, and the results showed that the sisal residue bio-oil is different from other bio-oils reported in the literature. It has high viscosity at room temperature, with a pour point of 55 °C and average molecular weight of 414.2 g/mol. In addition, phenolic species completely prevail in relation to the other monomeric components. The biochar obtained is an amorphous, fine powder. Despite the porosity, its specific surface area is lower than of commercial activated carbon.

1. INTRODUCTION

Sisal (*Agave Sisalana*) is a species of agave plant original from Mexico, and nowadays is spread throughout several continents. Its commercial exploitation is based on its fibers, whose physical characteristics (in particular, high resistance) justify its wide use in the automotive industry and ropes, craftworks, and papers production.[1] Accordingly, the total fiber production in the world in 2014 was 247 543 tons, from which 64.1 wt % were produced in the Americas, 31.3 wt % in Africa and 5.7 wt % in Asia.[2] In that same year, Brazil was the largest producer of sisal fibers, with 55.75% of its total production, immediately followed by The United Republic of Tanzania (11.94%), Kenya (8.90%), Madagascar (7.23%), China (5.53%), Haiti (4.21%), and Mexico (2.79%).[2]

Despite sisal fiber's importance in Brazil, its crop performance has been negatively affected in the past few years, mainly due to the reduction of planted areas and a decrease of productivity. These results are directly related to the high cost of production and low value paid for the fiber, mainly during the dry season.[3] The high production costs are intrinsically related to the lack of modern machines to harvest it, yielding only 4 wt % in terms of fibers.[4,5] Despite such difficulties, sisal is still one of the few economic options in semiarid regions in Brazil, where it is possible to find small family businesses. In that way, it is fundamental to find solutions that enable the fiber's competition with synthetic yarns by significantly reducing its production costs. In order to make the crop more attractive to rural producers, it is important that the defibration process is more efficient and that value is added to its residue. According to Fraga,[6] the processing of sisal residue is in an embryonic stage of exploitation, and its efficient use is directly dependent on the use of new technologies.

The bio-oil production from sisal's residue can be an interesting alternative in this context, being able to foster the technological development of the region and, consequently, contribute to the creation of new jobs in the rural environment.

Research on biomass conversion into bio-oil is moving the scientific and business environment around the world.[7−11] The possibility of extracting energy and chemical products from biomass for manufacturing purposes[12−17] strategically interests the government. Many leaders are aware of the possibility of developing areas located far from urban centers by using bio-oils. Combined with this, bio-oil is produced from renewable natural resources, which contributes to the reduction of pollutant emissions and is sustainable in the long term.[14,18]

Chemically, bio-oil resembles biomass in terms of elemental composition, being a complex mixture of polar organic compounds (75−80 wt %) and water (20−25 wt %), which may as well contain particles of the biochar.[8,13,19]

Fast pyrolysis is the main biomass conversion process for bio-oil production. According to Bridgwater,[20] the product yields can reach up to 75, 12, and 13 wt % for bio-oil, biochar and gas, respectively. The yields can vary depending on the type of biomass and applied conditions.[10] For instance, fast pyrolysis is characterized by the high heating rate of the particles to a temperature of about 500 °C, followed by a rapid cooling of the produced vapors in order to maximize the liquid fraction and suppress repolymerization and formation of noncondensable gases.[8] A fluidized bed reactor is the most common means of processing biomass in order to produce bio-oil.[21] Accordingly, the fluidization provides an excellent mixing between the particles, which makes the temperature uniform in the reactor and provides adequate conditions for the pyrolysis reaction.[22]

Received: May 16, 2018
Revised: July 26, 2018
Published: August 31, 2018

DOI: 10.1021/acs.energyfuels.8b01718
Energy Fuels 2018, 32, 9478−9492

Fast pyrolysis has been extensively used for bio-oil production from different lignocellulosic biomass. Sellin et al.[23] used banana leaves as feedstock, producing 49.6 wt % of gases, 27.0 wt % of bio-oil, and 23.3 wt % of the biochar. Moreover, these researchers identified complex phenolics and acids as products. Pradhan et al.[24] used Mahua seed (*Madhuca indica*) as raw material for the production of biofuels. The reaction was conducted in a semibatch reactor at 450−600 °C under a nitrogen atmosphere. The optimum reaction temperature was found at 525 °C, with a maximum yield of 49 wt % of bio-oil and 18 wt % of the biochar. The chemical characterization showed that the bio-oil contained a significant number of aliphatic and aromatic compounds. Carrier et al.[25] transformed sugar cane bagasse, corn cobs, corn stover, and Eucalyptus grandis into bio-oil. These researchers came to the conclusion that the biomass source influences the yields of pyrolytic water and organic species. Furthermore, lignin was suggested to inhibit the formation of pores in the biochars, while cellulose served as a precursor of the microporous character of the biochars. Asadullah and Rasid[26] produced bio-oil from palm kernel in a fluidized bed reactor. These authors reported that the higher rate of biomass feed and higher gas flow produced the highest yield of bio-oil. In addition, they observed that the bio-oil was biphasic when the reaction temperature was below 500 °C, and monophasic when the reaction temperature was above 500 °C.

The objective of this research was to evaluate the factors that influence fast pyrolysis of sisal residue in a fluidized bed reactor. This study was carried out in a fast pyrolysis pilot plant for the production of bio-oil, biochar, and noncondensable gases, whose yields were determined. The methodology was applied based on the statistical planning of experiments, where the operational variables were the reaction temperature, the nitrogen flow rate, and the biomass flow rate in the reactor. The test responses were the production of bio-oil rates, biochar and noncondensable gases. The sisal residue and pyrolysis products were further characterized in order to access their physical and chemical characteristics.

2. MATERIALS AND METHODS

2.1. Feedstock Preparation. The sisal residue was the raw material used in this research, and it was collected in the sisal region of Bahia in Brazil. It was produced from the scraping of sisal sheets in proper machinery to remove the fibers. The sisal residue was then stored in a freezer below 0 °C in order to avoid any degradation. A portion of the residue was dried in an oven at 105 °C for 4 h. After being cooled to room temperature, short sisal fibers were removed from the biomass, with only dried slices of the sheets remaining. The processed biomass had the same particle size distribution as the material produced in the field. Figure 1 shows the cumulative distribution of the sisal residue particle as determined by granulometric analysis. Sieve openings of 1/4−3/8 in. and 12 to 31/2 mesh sizes were used, and Sauter mean diameter was 0.89 mm.

2.2. Biomass Pyrolysis. *2.2.1. Pilot Pyrolysis Unit.* The bio-oil was produced through the process of rapid pyrolysis of the sisal residue in a pilot unit, as shown in Figure 2. The unit is composed of a silo of carbon steel (1) for the storage of biomass; a helical screw connected to an engine, which conducts biomass to the reactor; a bubbling fluidized bed reactor (2), made of stainless steel with 110 cm of height and 10 cm of diameter and surrounded by three electric resistances of 1300 W; two cyclones in series (3), constructed of stainless steel and thermally insulated, with glass collectors in their bases; a battery of four hull and tube capacitors (4) made of stainless steel, 90 cm long and 2.54 cm and 5.08 in inner and hull tube diameter, respectively, with glass collectors on their bases; and a

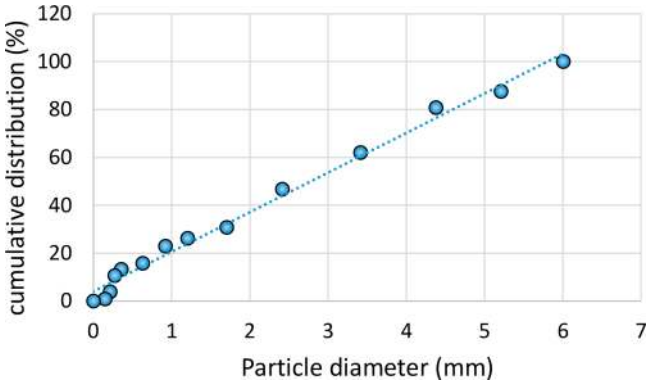

Figure 1. Distribution cumulative of biomass particle.

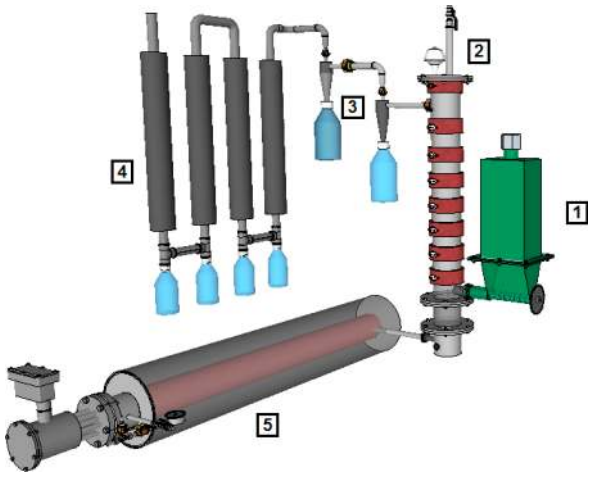

Figure 2. A blueprint of the pyrolysis machinery.

fluidizing gas heating furnace (5) of 13.5 kW, 140 cm long, and 21.4 cm in diameter (Anluz). The collection system also has two thermocouples located at the input of the first condenser and at the output of the fourth; the cooling fluid is water at a temperature of 9 °C, which ensures that the temperature of the noncondensable gases does not exceed 20 °C at the outlet of the fourth condenser. The unit also features a GC Chromatograph, Shimadzu brand, model GC-2014AT, ShinCarbon ST 100/120 mesh 2 m × 1 mm ID micropacked ID. In addition to this equipment, the pilot plant has a cold water unit with a cooling capacity of 5000 kcal/h, with a nominal flow rate of 1 m^3/h and a pressure of 30 m of water column (Metacontrol). The pilot plant has a maximum biomass consumption ratio of 2.5 kg/h.

2.2.2. Experimental Procedure. The dry biomass was stored in a silo (1), which was then hermetically sealed. After the furnace and reactor resistances were turned on, dry air was passed through the reactor at a flow rate of 15 m^3/h to fluidize the sand bed and promote the heating of the reaction medium up to the desired temperature. The data acquisition system continuously recorded the information regarding the temperatures along the reactor, pressure changes in the bed and the top of the reactor, in addition to the flow of the fluidizer gas. When the reaction temperature was reached, the fluidizer gas (i.e., dry air) was shifted to nitrogen, and the operating flow was adjusted. After 1 min of operation, the reaction medium was inert, and the biomass injection system was started. The reaction was considered completed after 1 h of operation. During the reaction, three products were obtained: bio-oil, biochar, and noncondensable gases. The bio-oil was collected in the heat exchangers, which are chilled with water at 9 °C, weighed, and stored in glass bottles at −2 °C; the biochar was collected, weighed, and stored in plastic bags; and two aliquots of the gas stream were collected, in order to identify the hydrogen, carbon monoxide, carbon dioxide, and methane present within the mixture.

DOI: 10.1021/acs.energyfuels.8b01718
Energy Fuels 2018, 32, 9478−9492

Table 1. Conditions Applied in the Fast Pyrolysis of Sisal Residue

test	nitrogen flow (Nm^3/h)	biomass flow (g/min)	reaction temperature (°C)	bio-oil yield (%)	biochar yield (%)	noncondensable gases yield (%)
1	8	10.33	450	12.68	37.17	50.14
2	14	10.33	450	13.65	29.43	56.93
3	8	25.95	450	12.22	48.36	39.42
4	14	25.95	450	9.94	42.93	47.09
5	8	10.33	550	8.03	23.23	68.73
6	14	10.33	550	5.52	29.81	64.57
7	8	25.95	550	11.60	26.59	61.77
8	14	25.95	550	14.49	34.68	50.83
9	11	18.55	500	17.41	47.05	35.54
10	11	18.55	500	15.92	46.33	37.74
11	11	18.55	500	16.58	50.80	32.62

The pyrolysis unit presented a biomass flow error in all the experiments. The granulometric distribution of the biomass varied from 0.15 to 6.0 mm (Figure 1), interfering randomly in the adequate filling of the helical screw and, consequently, in the amount of biomass that entered the reactor for the same flow. In addition to this problem, the reaction time varied according to the amount of nitrogen available. The actual mass was calculated by subtracting the mass placed in the silo before the reaction started (enough for 1 h of reaction) from the mass remaining in the silo after the process.

2.2.3. Experimental Planning. The experiments were defined using the experimental planning technique, with the objective of investigating the effects of the operational variables of the pyrolysis process on bio-oil production. According to Choi et al.[18] and Bridgwater,[10] the distribution and composition of the fast pyrolysis products can be strongly influenced by the following variables: reaction temperature, inert gas flow, biomass flow, particle sizes of biomass and sand and cooling temperature.

The granulometric distribution was kept constant in all tests due to the premise of this work, which was to use the biomass with the same granulometric distribution as the sisal leaf defibration process. The silica sand mass, inserted into the reactor as an inert fluidizing element, and the average diameter of this same material were kept constant (4 kg and 0.425 mm, respectively). These values were measured in preliminary tests, since they are the most adequate to keep the bed temperature constant. The type of fluidizing gas (nitrogen) was kept constant for economic reasons. The reaction time varied according to the nitrogen flow of each test due to the capacity of the nitrogen cylinder to keep the flow constant. The temperature and flow of the refrigerant (water at 9 °C and 0.1 m^3/h) were kept constant because these values were the most adequate to cool the pyrolytic gases, which were cooled from approximately 220 to 21 °C, favoring the collection of bio-oil.

In this research, nitrogen gas flow, biomass flow rate, and reaction temperature were considered the most influential variables of the pyrolysis process, and, consequently, their effects on bio-oil production were investigated. The reaction temperature directly influences pyrolysis chemical products.[27] The temperatures used in this work were defined based on the optimum values found for the pyrolysis of several biomasses and have already been published in the literature.[28] For this reason, the tests involved temperatures of 450, 500, and 550 °C.

The biomass mass flow rates injected into the reactor were chosen based on the maximum rotation of the motor connected to the helical screw used in the pyrolysis unit. The values of the rotations allowed in this work were 20, 30, and 40 rpm, which equals the injection of 10.33, 18.15, and 25.95 g/min of biomass, respectively.

The fluidization of the system occurred from commercial nitrogen injection in 9 m^3 cylinders. The fluidization gas flow rates used were 8, 11, and 14 N m^3/h, whose values were defined between the initial fluidization flow and the drag flow of the particles. In this case, the residence time of pyrolytic vapor varied between 2.07 and 3.88 s, depending on the reaction temperature.

Table 1 shows the tests performed and the results of bio-oil yield, biochar, and noncondensable gases. The mass of noncondensable gases was determined by the difference between the mass of biomass reacted and the sum of the bio-oil mass.

The tests were designed according to the experiments planning technique with three independent variables (nitrogen flow, biomass flow, and reaction temperature) and two values for each of them, resulting in the conditions 1−8. In order to determine the variability of the experimental responses in bio-oil production, three additional tests were performed with the intermediate values of all the variables (tests 9, 10, and 11).

2.2.4. Composition of Noncondensable Gases. The composition of the noncondensable gases was defined through a GC-2014 gas chromatograph (Shimadzu). It was equipped with a thermal conductivity detector (TCD), model TCD-2014 and a ShinCarbon ST 100/120 mesh column (2 m × 1 mm ID micropacked). The carrier gas was helium, with a flow rate of 10 mL/min. The temperatures of the injector and detector were 100 and 200 °C, respectively.

The chromatograph was calibrated to identify the volumetric fraction of nitrogen, carbon monoxide, carbon dioxide, and methane, which are the most abundant noncondensable gases produced by pyrolysis.[29]

The mass of these gases were determined from the following steps:

(i) Calculation of the total volume of noncondensable gases from each test:

$$V = \frac{V_{N_2}}{y_{N_2}} \tag{1}$$

where V_{N_2} and y_{N_2} are the volume of nitrogen used in each test and the volumetric fraction of the nitrogen found a from the chromatograms, respectively.

(ii) Calculation of the volume of each gas:

$$V_i = y_i V \tag{2}$$

where y_i and V are the volumetric fraction found from the chromatograms and the total volume of each test calculated in step *i*, respectively.

(iii) Calculation of the mass of each gas:

$$m_i = V_i \mathrm{PM}_i \tag{3}$$

where V_i and PM_i are the volume calculated in step *ii* and their molecular weight, respectively.

(iv) Calculation of the total mass of the gases:

$$m_T = \sum m_i \tag{4}$$

where $\sum m_i$ is the sum of the mass of each gas without the nitrogen mass.

(v) Calculate the total mass of the gases not analyzed by the chromatography for each test (called others) from the

DOI: 10.1021/acs.energyfuels.8b01718
Energy Fuels 2018, 32, 9478−9492

Table 2. Physical and Chemical Characteristics of Biomasses

characteristics	sisal residue	banana leaves Sellin et al.[23]	Eucalyptus Crandis Oasmaa et al.[9]	sugar cane bagasse Carrier et al.[25]	Mahua seed Pradhan et al.[24]
Biochemical (wt %)					
cellulose	12.26	26.7	∼20	44.2	32.4
hemicellulose	1.13	25.8	∼51	23.8	7.9
lignin	20.87	17	∼27	22.4	29
physical property					
particle size (mm)	1−2	<1 (80%)	3−5	0.25−2	0.55−1
bulk density (kg/m^3)	140			170	
high heating value (kJ/kg)	16700	17100	19900	17600	26690
proximate analysis (wt %)					
water	6.11	7.8	7.6	6.7	8.6
volatile	82.40	78.2	82.7	76.1	84
fixed carbon	1.31	15.6		6.9	5.4
ash	16.28	6.2	0.4	9.1	2.0
Ultimate analysis (wt %)					
C	50.3	46.8	50.0	49.8	61.7
H	5.8	6.7	6.0	6.6	8.4
O[b]	42.4	45.6	44.0	43.0	25.7
N	1.5	0.9	0.1	0.6	4.2
O/C	0.63	0.73	0.66	0.65	0.31
H/C	1.38	1.72	1.44	1.59	1.63

subtraction of the total mass of the gases that were not condensed (determined by the subtraction of the biomass mass flow by the sum of the bio-oil and biochar) by the sum of the gas mass flow rates calculated in step *iv*.

2.3. Characterization of Biomass and Its Products.

2.3.1. Chemical and Physical Analysis. Sisal residue, bio-oil, and biochar were characterized by chemical and physical analyses. Moisture, volatile matter, and ash were determined by proximate chemical analysis using thermogravimetry (dried in oven and burnt in muffle furnace) according to procedures described, respectively, in the ASTM E871-82, ASTM E872-82, and ASTM E1755-01 standards. All procedures were carried out in triplicate. Fixed carbon was determined using the data previously obtained in the proximate analysis. The ultimate analysis of carbon, oxygen, hydrogen, nitrogen, and sulfur weight percentages of biomass, bio-oil, and biochar were determined from CHNSO elemental analysis (628 Series, LECO). The Silva and Queiroz method was performed to determine the concentrations of cellulose, hemicellulose, and lignin of the biomasses, and the procedure is detailed in the literature.[30]

An oscillating U-tube density and sound analyzer (DSA 5000, Anton Paar, Austria) were used to measure the densities of the bio-oil at 60 °C.

The calorific values of sisal residue and its pyrolysis products were estimated using a bomb calorimeter (model: 6400 Calorimeter, Parr) in which a 0.5 ± 0.05 g sample was placed inside the bomb and burned in the presence of oxygen. An increment of ±0.01 °C accuracy was used to determine the gross heating value (GHV) as in the procedure ASTM D 4809-95.

2.3.2. XRF Analysis. This study was done on a wavelength-dispersive XRF spectrometer (S8 Tiger from Bruker AXS delivered in 2009) with a 4 kW water-cooled X-ray tube with a Rh anode, a 75 μm Be window, and a 60 kV maximum acceleration voltage. Spectrum recording and evaluation were performed with the precalibrated/standardless software Quant-Express (Bruker AXS, delivered with the XRF instrument), intended for the analysis of approximately 70 elements from F to U.

2.3.3. Thermogravimetric Analysis. The thermogravimetric analyses of sisal residue were performed on a Shimadzu TGA/DTA analyzer model TGA-50. Samples of approximately 1.5 mg were heated until 1000 °C at a heating rate of nitrogen of 10 °C min^{-1}. The analyses were carried out in triplicate in order to observe the results' reproducibility. The mass loss (TG) and differential weight loss (DTG) were obtained using the analyzer software.

2.3.4. FT-IR spectroscopy. Functional groups of the bio-oil were identified using Fourier transform infrared (FT-IR) spectroscopy, and the analyses were performed on an attenuated total reflection infrared (ATR-IR) spectrometer. Around 1−2 drops of sample were placed on the sample unit (Graseby Specac Golden Gate with diamond top), and IR-spectra were obtained using a Shimadzu IR Tracer-100 FT-IR spectrometer with resolution of 4 cm^{-1} and 64 scans.

2.3.5. Molecular Weight. Gel permeation chromatography (GPC) was used to determine the relative molecular weight distribution (relative to polystyrene standards) of the bio-oil constituents. GPC analyses were performed using an Agilent HPLC 1100 system equipped with a GBC LC 1240 refractive index detector. For the GPC analyses, the eluent for the phenolic oligomers was tetrahydrofuran (THF) with three PLgel 3 μm MIXED-E columns in series (length: 300 mm; internal diameter: 7.5 mm). The column flow rate and temperature were 1.0 mL min^{-1} at 25 °C. Polystyrene was used as a calibration standard. Average molecular weight calculations were performed using the PSS WinGPC Unity software from Polymer Standards Service. The samples were prepared by using 4 mL of THF, 2 drops of toluene as the flow marker, and 0.05 g of the bio-oil. All samples were filtered with a filter pore size 0.2 μm before injection.

2.3.6. NMR Spectroscopic Analysis. NMR analyses were performed on bio-oil with the sample being dissolved by 50 wt % with dimethyl sulfoxide-d_6 (DMSO-d_6). Heteronuclear single quantum coherence (HSQC) spectra were obtained from a Varian Unity Plus operating at a frequency of 400 MHz. The HSQC spectra were recorded using 11 ppm sweep width in F2 (1H), 220 ppm sweep width in F1 (13C), 8 scans, 1024 increments, and a total acquisition time of around 6 h.

2.3.7. GC-MS Spectroscopic Analysis. Gas chromatography/mass spectrometry (GC-MS) analyses were performed on a Hewlett-Packard 6890 gas chromatograph equipped with a Quadrupole Hewlett-Packard 5973 MSD selective detector attached (split ratio of 1:50). The analytes were separated in a chromatographic column Restek Rxi-5Sil capillary (length: 30 m; internal diameter: 0.25 mm; thickness of stationary phase: 0.25 μm). Helium was used as carrier gas (flow of 1 mL min^{-1}). The injector temperature was set at 280 °C. The oven temperature was kept at 40 °C for 5 min, then increased to 250 °C at a rate of 3 °C min^{-1}, and held at 250 °C for 10 min. All samples were diluted around 25 times with a 500 ppm solution of di-*n*-butyl ether (DBE, internal standard) in THF. Spectral interpretation was carried out using the NIST MS Search program (Version

DOI: 10.1021/acs.energyfuels.8b01718
Energy Fuels 2018, 32, 9478−9492

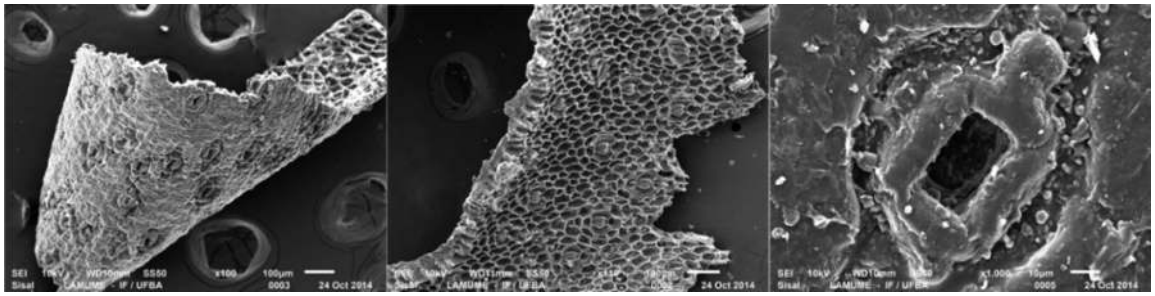

Figure 3. SEM image of sisal residue.

2.0) operating on the NIST/EPA/NIH Mass Spectral Database 2011 (NIST 11).

3. RESULTS

3.1. Biomass Characteristics and Properties. The physical and chemical characteristics of dried sisal residue are presented in Table 2, together with results of other biomasses as reported in the literature.

The sisal residue presents distinct physical and chemical characteristics when compared to other biomasses as observed in Table 2. The cellulose and hemicellulose contents of the sisal residue are low in relation to most of the plant biomasses, which normally contain more than 20 wt % of cellulose and more than 15 wt % of hemicellulose. The lignin content of the sisal residue is in the range of most plant biomasses.[31] The sum of the contents of cellulose, hemicellulose, lignin, and water contained in the sisal residue (40.37 wt %) is very low in relation to other biomasses (for example, 69.5 wt % of banana leaves), as well as the oil content (4.14 wt %), implying the existence of high levels of extractives and inorganic species. Reduced levels of cellulose and hemicellulose in biomass produce heavier oils because they contain lower amounts of sugar-derived low molecular weight compounds (i.e., levoglucosan, acetaldehyde, organic acids) and higher amounts of large aromatic fragments derived from lignin.[8]

The moisture content of the sisal residue was of 6.11 wt %, which is compatible with the levels reported for other biomasses. According to Bridgwater (2012), the dry biomass must have a maximum moisture value of 10 wt %. In this way, it will have a small effect on conversion efficiency.[24]

The sisal residue has a very high volatility of 82 wt %, which indicates that good yields of liquid and noncondensable gases are achievable. However, the high content of ash (16 wt %) may have negative impacts on bio-oil production and quality because its alkali metals, such as potassium and sodium, cause secondary cracking of vapors.[10] The X-ray fluorescence spectrometry, for example, performed to determine some impurities present on the sisal residue, identified the following species: Ca, Mg, K, Si, Fe, P, Al, Zn, Sr, Na, and Cl.

The sisal residue presents high content of carbon (41.23 wt %), hydrogen (4.77 wt %), and oxygen (34.76 wt %). However, high amounts of nitrogen (1.25 wt %) and sulfur (1.71 wt %) were found in relation to other plant biomasses.[9] These values were attributed to the soil characteristics where the sisal palm grew. The high values of nitrogen and sulfur found in the sisal residue can form high amounts of sulfur and nitrogen oxide, which are toxic and corrosive species.[23]

The composition of the sisal residue contains typical lignin content and extractives, resulting in an O/C of 0.63 and an H/C of 1.38, values compatible with those of other vegetal biomasses and which gives the biomass products a high energy value.[9]

The morphology of the sisal residue was analyzed by scanning electron microscopy (SEM). The obtained micrographs are shown in Figure 3, and it can be observed that the sisal residue has a porous structure with alveolar and flat appearance and with size and shape characteristic of the sisal leaf defibration process, containing pores of varied geometry.[32] In addition, it is possible to notice a rigid structure, due to the vegetal cell structure, composed of fibrocells typical of forage species.[33,34] The cellular plant structure of sisal is composed of fibrocells, lignin, and hemicellulose, presented in cell walls, in addition to lumens. It is believed that this type of structure will benefit the production of bio-oil due to the rapid transfer of heat through the material.

The thermal degradation and conversion profile of the sisal residue was determined by TGA/DTG in order to understand the pyrolytic yield of biomass. Figure 4 shows the correlation

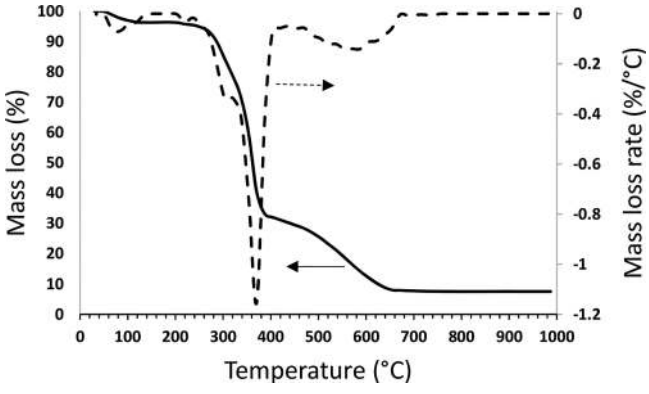

Figure 4. Thermogravimetric analysis of sisal residue.

between weight loss of the sisal residue and temperature (TGA) and also peaks whose areas are proportional to the mass variation of the sample as a function of temperature (DTG). The TGA/DTG curves exhibits four main stages: (i) moisture drying—the peak observed from room temperature to approximately 220 °C indicates the evaporation of moisture from dry biomass and decomposition of extractives; (ii) the degradation of hemicellulose occurred from approximately 220−320 °C; (iii) the degradation of cellulose and part of lignin occurred around 320−437 °C; (iv) degradation of larger lignin fragments took place at around 437−688 °C.

The four stages found are in accordance with the work of Raveendran et al.,[35] as well as the thermal behavior observed. These authors studied the thermal degradation profiles of 14 types of biomasses, as well as those of their components. It was

DOI: 10.1021/acs.energyfuels.8b01718
Energy Fuels 2018, 32, 9478−9492

observed that the main degradation of the hemicellulose fraction occurred between 250 and 350 °C, while the cellulose has its main degradation between 350−500 °C, when part of the lignin also begins to degrade. The main degradation of lignin, however, occurred at temperatures above 500 °C. In the present study, the pyrolysis temperatures applied were of 450−550 °C, a range in which high thermal degradations (i.e., 70−80 wt %) could be observed in the TGA/DTG analyses. Therefore, the fast pyrolysis process in fluidized bed is expected to produce the maximum volatilization of biomass under such temperatures.

Figure 5 shows the FTIR spectrum of the sisal residue. A broad and intense band centered at 3348 cm^{-1} can be

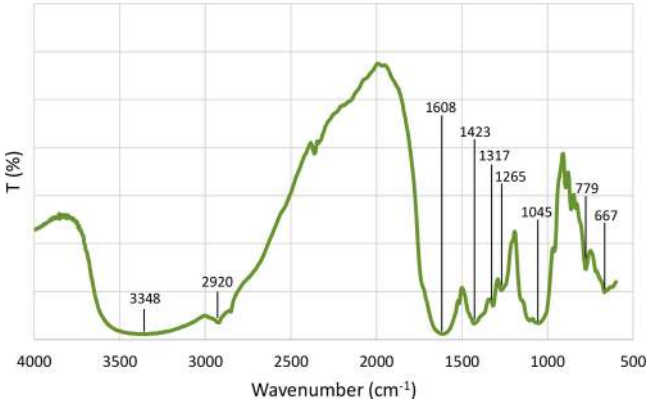

Figure 5. FTIR of sisal residue.

observed, and it relates to the stretching vibrations of the O−H bonds of phisisorbed water.[36] It can be also observed a band at 2920 cm^{-1}, attributed to the stretching of the C−H bond of methyl and methylene groups, common in lignocellulosic materials.[36,37] The band observed at 1608 cm^{-1} is characteristic of the vibrational stretching of the C═C aromatic bond.[38] On the other hand, the vibration at 1423 cm^{-1} may be associated with the deformation of the C−C bonds of aromatic rings.[39] It is also observed that one point at 1265 cm^{-1} refers to the stretching of the C−O bond of the pyran ring.

3.2. Pyrolysis Products. *3.2.1. Bio-Oil.* The relationship between the bio-oil yield and the operational conditions (i.e., volumetric flow rate of N2 (1), biomass mass flow (2) and reaction temperature (3)) is complex, and the best way to evaluate it is by studying the interaction effects using statistical design.[40] Therefore, the Response Surface Methodology (RSM) was chosen for this study.[40−42] This approach consists of a group of statistical techniques that allows a reduction in the number of experiments and a prediction of the influence of the factors on the chosen response using a mathematical model. The latter can be graphically represented with response surfaces that show the extent of the influence of the parameters or whether their interactions are significant and can then be used to provide the optimal conditions to improve a process. The best approach for comparing various measures is the analysis of variance (ANOVA).[40−42] ANOVA is the statistical treatment most commonly applied to experimental results in order to determine the contribution of each parameter. Accordingly, ANOVA provides the significance of all main factors and their interactions by comparing the mean square against an estimate of the experimental errors at specific confidence levels. The significance of the RSM model is shown in Table 3, as well as the degree of freedom, sum of squares, contribution of each parameter in the prediction model,

Table 3. ANOVA Results for the Mass Flow of Bio-Oil[a]

	variables			
	(SS)	(df)	(MS)	P
2	8.7425	1	8.7425	0.058200
3	9.7883	1	9.7883	0.052462
2 by 3	34.8967	1	34.8967	0.015588
lack of fit	10.4008	4	2.60020	0.184115
pure error	1.1139	2	0.55695	
total SS	133.9208	10		
R^2	0.91			
R^2 adj	0.86			

[a](1) Volumetric flow rate of N_2; (2) biomass mass flow; (3) reaction temperature.

modified sum of the squares, modified average sum of the squares, and *P*-value for each parameter as a result of the performed analysis of variance. A lower *P*-value is attributed to a higher importance of that factor and model. *P*-values lower than 0.1 (i.e., confidence level of 90%) indicate that the studied parameter is significant in the results of the model. *P*-values greater than 0.1, as observed for the main variable (i.e., volumetric flow rate of N_2 (1)) and first order interactions (i.e., volumetric flow rate of N_2 (1)/biomass mass flow (2) and volumetric flow rate of N_2 (1)/reaction temperature (3)), indicate that null hypotheses were acceptable and that the effects of those variables were removed from the calculation. *P*-values much lower than 0.1, as in the case of the other response variables, indicate that those parameters were important. The coefficient of determination (R^2) indicated how well the variation in response (i.e., bio-oil yield) was explained by the model. Larger values of predicted R^2 suggest models of greater predictive ability. The model gives a better prediction of the mass flow of bio-oil when the regression coefficient is close to unity, as shown in Table 3 (0.91). Adjusted R^2 (R^2 adj) accounts for the number of predictors in the model and is useful for comparing models with different numbers of predictors. Table 3 shows that R^2 adj = 0.86 when nonsignificant variables were removed from the model, becoming more suitable to predict the mass flow of bio-oil. Pure-error and lack-of-fit are parts of the residual sums of squares that are relevant for testing a hypothesis. For instance, the pure-error is the part that cannot be predicted by any additional terms, while lack-of-fit can be predicted by including additional terms for the variables in the model. Table 3 shows a nonsignificant *P*-value (>0.1) for lack-of-fit, becoming thus more suitable to predict the yield of bio-oil. The calculated mean square pure error of 0.56 indicates that the observed values by the model had low variability compared to the average.

The combined effects of the flow rate of biomass and reaction temperature were investigated to obtain the bio-oil yield, as shown in Figure 6a. It was observed that the flow rate of biomass strongly interacts with the temperature, presenting a higher yield region of bio-oil at temperatures below 500 °C and flow rate of biomass over 18 g/min. However, the highest yields were achieved for the lowest reaction temperature, regardless of the biomass flow rate, and for the higher biomass flow rate, regardless of the reaction temperature.

DOI: 10.1021/acs.energyfuels.8b01718
Energy Fuels 2018, 32, 9478−9492

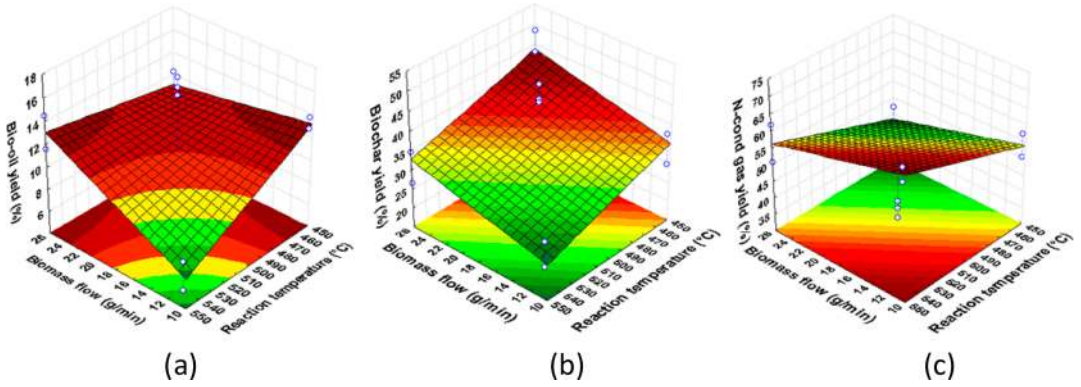

Figure 6. Response surface representing the combined effects of variables on the yield: (a) bio-oil; (b) biochar; and (c) noncondensable gas.

When the pyrolysis temperature was set to below 500 °C, it is possible that there has been little influence of secondary reactions such as cracking, repolymerization, and recondensation to maximize bio-oil yield.[26]

The increase of biomass flow rate caused a decrease in the solid-to-solid heat transfer rate and, consequently, the decrease in the primary volatile formation, increasing the yield of bio-oil.[26] This effect is in agreement with the surface behavior shown in Figure 6, that even at temperatures above 500 °C, bio-oil production increases with increasing biomass flow rate due to the decrease in the solid-to-solid heat rate. In addition, increasing the biomass flow rate increased the residence time of the organic molecules,[43] contributing to the increase and decrease of the yields of heavy and light fractions, respectively.[44] Bio-oil of the sisal residue has characteristics of heavy bio-oil (Figure 7), the formation of which derived partially from lignin,[44] which is the most abundant polymer of the sisal residue (Table 2). The bio-oil yields have been reported in the literature as light and heavy fractions.[43−52] Table 4 shows that the heavy bio-oil yield varied between 14.3% and 79%, depending on the type of biomass and variation of pyrolysis temperature. Although the higher yields of the sisal residue bio-oil are in the range of heavy fractions, the absence of the aqueous phase is not common in relation to those produced by another biomass. According to Pereira and Pires,[43] the bio-oil produced from sisal residue had high viscosity at room temperature due to the chemical characteristics of the biomass.

Figure 7. Bio-oil of sisal residue.

3.2.2. Biochar Production and Noncondensable Gases. The combined effects of the flow rate of biomass and reaction temperature also were investigated to obtain the biochar and noncondensable gases yield, as shown in Figure 6, panels b and c, respectively. The highest biochar yields were achieved for the lowest reaction temperatures and for the higher biomass flow rates. However, the highest noncondensable gases yields were achieved for the higher reaction temperatures and for lowest the biomass flow rates. The trend of biochar and noncondensable gases yields is consistent with the performance of bio-oil yield explained in Section 3.2.1.

Fast pyrolysis is a thermoconversion process that favors the production of bio-oil by preventing the formation of the biochar and noncondensable gases. Nevertheless, depending on the operational conditions of the pyrolysis, it is possible to combine the production of bio-oil with the other products in

Table 4. Light and Heavy Fraction of Bio-Oil

			yield (%)				
biomass	moisture (%)	temperature (°C)	heavy bio-oil	light bio-oil	biochar	gas	ref
banana leaves	7.8	500	17	10	23.3	49.6	Sellin et al.[23]
Mahua seed	8.6	450	33	24	26	18	Pradhan et al.[24]
palm kernel shell	12	550	50	32−34	32	15	Asadullah et al.[26]
cassava rhizome	10.5	600	19	10	55	16	Zhang et al.[44]
corn stalk	10.2	700	15.7	9.4	55	12.5	Zhang et al.[44]
beech wood	10.6	495	14.3	23	14.7	13.4	Jendoubi et al.[45]
neem seed	16	450	37		36	25	Nayan et al.[46]
Karanja seed	15.2	450	42.5		34	18	Nayan et al.[47]
sugar cane	10.4	600	16.8	15	28.6	42.6	Mesa-Pérez et al.[48]
sal seed	8.46	450	37		32	31	Singh et al.[49]
Mahua seed	5.65	500	52.5	22	23	24	Shadangi and Mohanty[50]
Kaner seed	4.3	600	79	2.2	10	9	Gouda et al.[51]
hornbeam sawdust	8.78	500	29		25	22	Morali et al.[52]

DOI: 10.1021/acs.energyfuels.8b01718
Energy Fuels 2018, 32, 9478−9492

order to use them as raw material for the generation of value-added chemical products. Accordingly, biochar (C) and noncondensable gases (H_2, CO, CO_2, CH_4, and others) can be used as fuel.[10] In addition to this application, biochar can be converted into activated carbon, and the noncondensable gases can serve as a source of synthesis gas. The further use of the noncondensable gases is clearly dependent on the efficient separation of the gases of interest, such as H_2, CO, and CH_4. The yields of the biochar and noncondensable gases from the pyrolysis experiments are shown in Table 1 and Table 5.

Table 5. Yield of Noncondensable Gases

test	hydrogen (%)	carbon moxide (%)	carbon dioxide (%)	methane (%)	others (%)
1	2.13	33.78	0.00	3.87	10.36
2	0.00	0.00	13.26	0.00	43.66
3	0.00	0.00	0.00	0.00	39.42
4	10.10	2.85	17.73	0.66	15.76
5	0.58	2.03	10.94	0.00	55.17
6	0.48	35.24	4.36	6.29	18.20
7	0.00	3.74	0.00	0.00	58.03
8	16.11	7.44	8.90	0.50	17.88
9	0.06	11.46	15.59	0.88	7.55
10	0.00	14.43	17.19	0.94	5.18
11	0.50	13.28	17.02	1.54	0.28

The highest bio-oil yields were observed in tests 2, 8, and central point. Although the central point produced the highest yield of bio-oil, test 8 produced one of the lowest biochar yields and one of the highest H2/CO ratios (i.e., 2.16), which is suitable for the production of methanol and liquid biofuels.[53] As expected, the milder operating conditions of test 2 led to lower amounts of the biochar and noncondensable gases.

3.3. Analysis of Pyrolysis Products. In item 3.2, we investigated the influence of some operational variables on the production of bio-oil in order to identify the best conditions within the evaluated range that provides the highest bio-oil yields. To further achieve maximum bio-oil production, an optimization study would have to be done, which is not in the scope of this paper. For this reason, test 8 was chosen as a reference due to the largest H_2/CO rate and for producing one of the highest bio-oil yield. Its liquid and solid products were further characterized.

3.3.1. Bio-Oil Characteristics and Properties. The bio-oil traditionally has two liquid phases: one aqueous and the other oily. The aqueous phase is called light bio-oil (pyroligneous acid) and has low viscosity, while the oil phase has a higher viscosity.[23] Remarkably, the bio-oil of the sisal residue has a greasy aspect, as shown in Figure 7, having a pour point of 55 °C and a viscosity that can reach 2500 mPa·s at 60 °C.[11] On the other hand, bio-oils from other biomasses flow at room temperature (Table 6) and have a viscosity in the range of 100 mPa·s and 400 mPa·s at 40 °C.[10]

The bio-oil of the sisal residue exhibits distinct physical and chemical characteristics from many bio-oils reported in the literature but shares similarities with the Mahua seed bio-oil, as shown in Table 6. The bio-oil density of the sisal residue at 25 °C was 921.52 kg/m^3, which is relatively close to the density of heavy fuel oil, which has a typical value of approximately 855 kg/m^3.[26]

The water content of the sisal residue was of 5.18 wt %, which is a low value compared to other bio-oils. According to

Table 6. Characteristics of Bio-Oil

characteristics	sisal residue	banana leaves Sellin et al.[23]	Eucalyptus Crandis Oasmaa et al.[9]	Pine saw dust Oasmaa et al.[9]	Mahua seed Pradhan et al.[24]
Physical property					
bulk density (kg/m^3)	921.5		1229	1206	921.3
high heating value (kJ/kg)	35331	25000	17000	16900	39020
pour point (°C)	55		−42	−36	
proximate analysis (wt %)					
water	5.18		20.6	23.9	1.1
ash	1.06		0.03	0.03	
Ultimate analysis (wt %)					
C	72.7	56.0	42.3	40.6	69.9
H	9.6	7.8	7.5	7.6	9.2
O	15.3	35.3	50.1	51.7	18.3
N	2.4	0.90	0.1	<0.1	2.6
S	0.6	0.08	0.02	0.01	0.89
O/C	0.16	0.47	0.89	0.95	0.20
H/C	1.58	1.67	2.13	2.25	1.58

Duanguppama et al.,[54] the increase in terms of viscosity of bio-oils is caused by water reduction and high concentration of water-insoluble components during the pyrolysis reaction. Therefore, the relatively low amount of moisture contributed to the increase of the viscosity of the bio-oil of the sisal residue, which consequently generated a pour point of 55 °C. In addition, the ash content was high compared to other bio-oils, which is likely to contribute to the high pour point observed.

The bio-oil of the sisal residue exhibits high carbon content (72.7 wt %), an amount of hydrogen close to other bio-oils (9.6 wt %), and a low amount of oxygen (15.3 wt %). The carbon and hydrogen contents of the bio-oil of the sisal residue are very close to those found in heavy fuel oil (~83 and 10 wt %, respectively); however, the oxygen content of the bio-oil of the sisal residue is still very high relative to petroleum.[55]

The bio-oil of the sisal residue presents O/C and H/C ratios of 0.16 and 1.58, respectively. The O/C value of the bio-oil of the sisal residue is still very high in comparison with petroleum, but lower when compared with most bio-oils. The lower oxygen content is probably due to the conversion of more oxygen into noncondensable gases during pyrolysis.[24] Nevertheless, the H/C value is very close to the value found for petroleum. The high H/C ratio was mainly responsible for the high value of high heating value (35 331 kJ/kg).

The percentage of nitrogen and sulfur in the bio-oil can be an indication of whether the fluid can pollute the environment during its combustion. The bio-oil of the sisal residue has high amounts of nitrogen (2.33 wt %) and sulfur (0.6 wt %) in comparison with other bio-oils, as observed in the Mahua seed bio-oil. According to Sellin et al.,[23] high amounts of sulfur and nitrogen oxide make the material toxic and corrosive.

The determination of the main functional groups of the bio-oil of the sisal residue was possible through the interpretation of FTIR spectra, which are shown in Figure 8, which show observed peaks from 3500 to 650 cm^{-1}, represented in Table 7.

DOI: 10.1021/acs.energyfuels.8b01718
Energy Fuels 2018, 32, 9478−9492

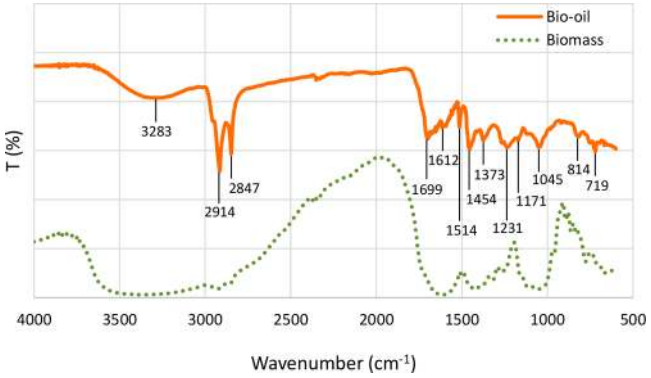

Figure 8. FTIR spectra of sisal residue and its respective bio-oil.

Table 7. FTIR Functional Group and Type of Vibration

wavelength range (cm^{-1})	frequency (cm^{-1})	functional group	type of vibration
3600−3200	3283	water, phenols, carboxylic acids, water impurities, alcohols	O−H stretching
3000−2800	2914, 2847	alkanes	C−H stretching
1750−1650	1699	ketones, ester and aldehyde groups	C−O stretching
1600−1450	1454, 1514	alkene, aromatics	C═C stretching
1300−950	1231, 1171, 1045	alcohols, phenols, ethers and esters	C−O stretching
900−690	814, 719	mono- and polycyclic and substituted aromatic groups	O−H bending

The broad peak observed between 3600 and 3200 cm^{-1} relates to the O−H stretching vibration and can be attributed to water, phenols, carboxylic acids, water impurities, and alcohols in bio-oil.[24,26] The peaks between 3000 and 2800 cm^{-1} were attributed to the presence of alkanes due to the symmetric and asymmetric stretching vibrations of aliphatic C−H bonds in the CH3 and CH2 groups.[26,27] The band between 1750 and 1650 cm^{-1} was assigned to C═O stretching vibrations and indicates the presence of ketones, esters, and aldehyde groups.[27] The following band in the range of 1650 and 1580 cm^{-1} represents the aromatic group.[26] The C═C stretching vibration between 1600 and 1450 cm^{-1} indicates the presence of alkene and aromatics.[24] On the other hand, the C═C stretching vibration between 1550 and 1490 cm^{-1} can be attributed to nitrogen compounds which describe $-NO_2$ stretching and NH bending.[27] The peaks between 1300 and 950 cm^{-1} were attributed to alcohols, phenols, ethers, and esters due to the C−O stretching vibrations and O−H deformation vibrations.[26] The bands between 900 cm^{-1}−690 and 1450 cm^{-1}−1350 cm^{-1} were assigned to O−H bending, which indicated the presence of aromatics groups.[26] In addition, the peaks in between 1470 and 1365 cm^{-1} were attributed to asymmetric and symmetric C−H bending of methyl, particularly alkanes, including gem-dimethyl and *tert*-butyl groups.[27] These compounds were also observed for other bio-oils produced from palm kernel shell,[26] banana leaves,[23] and Mahua seed.[24]

The molecular weight distribution of the bio-oil of the sisal residue is shown in Figure 9. The bio-oil GPC profile shows distributions of molecular weights from 100 M_w to over 1000 M_w, with three peaks with maxima at approximately 250 M_w and 450 M_w and 750 M_w, and polydispersity index (PDI = M_w/M_n) of 1.42. These results indicate that the bio-oil consists of a wide range of fragments, including significant amounts of monomers, dimers, trimers, and tetramers, as well as high molecular weight oligomers. Through the spectrum, it was possible to observe that 63% of the bio-oil compounds have a molecular weight less than 400 g/mol, and only that portion can generally be detected by phase chromatography.[56] The sisal residue bio-oil exhibited a weight-average molecular weight (M_w) of 414.2 g/mol and a number-average molecular weight (M_n) of 291.5 g/mol. The average molecular weights, M_w and M_n, of the bio-oil produced were slightly lower than those of the pyrolytic lignin obtained from palm kernel shells.[57]

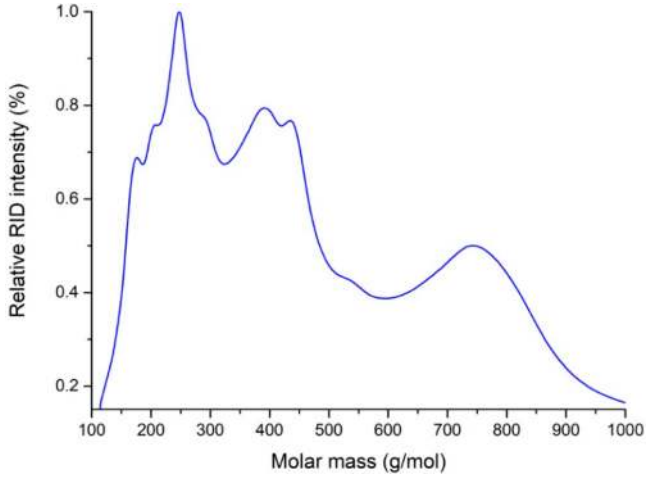

Figure 9. GPC analysis of sisal residue bio-oil.

The sisal residue bio-oil was characterized by 2D NMR HSQC to facilitate the elucidation of its large fragments, which are not detectable by GC.[58]

The spectrum can be divided into three main regions and interpreted qualitatively. Figure 10 shows the 2D NMR spectra and the aliphatic region ($\delta C/\delta H$ 10−48/0.5−2.75 ppm), oxygenated aliphatic region ($\delta C/\delta H$ 52.5−90.0/2.8−5.7 ppm), and aromatic region ($\delta C/\delta H$ 105−155/6.0−9.2 ppm), according to the work published previously by Mattsson et al.[59]

The aliphatic region mainly consists of C−H bonds from alkanes derived from the deoxygenation of biomass during pyrolysis, as well as alkyl and allyl side chains from aromatic and phenolic structures (i.e., methyl phenol). The oxygenated aliphatic region is composed of C−H bonds close to ether, hydroxy, and carbonyl groups as in ketones and sugar molecules, mainly from the cellulose and hemicellulose fractions of the sisal residue. Besides these groups in this spectral region, methoxy side groups from aromatic structures such as guaiacols are well separated and can be clearly identified. The aromatic region consists basically of lignin-derived aromatic and phenolic structures present within the bio-oil. Oligomers derived from the lignin residue of sisal and by guaiacil (G) rings, units: C2−H2 with a signal at 110.9/6.99 ppm; C5−H5 at 114.9/6.72, and 6.94 ppm and C6−H6 at 118.7/6.77 ppm.[60,61] In addition, guaiacil generated only one signal, of three possible, suggesting that G units have a high degree of substitution. A signal related to C═C bonds as in alkenes can be also clearly visualized.

In Figure 11 the main structures of the (a) aliphatic, (b) oxygenated aliphatic, and (c) aromatic regions present in the bio-oil of the sisal residue are represented. Table 8 shows a

DOI: 10.1021/acs.energyfuels.8b01718
Energy Fuels 2018, 32, 9478−9492

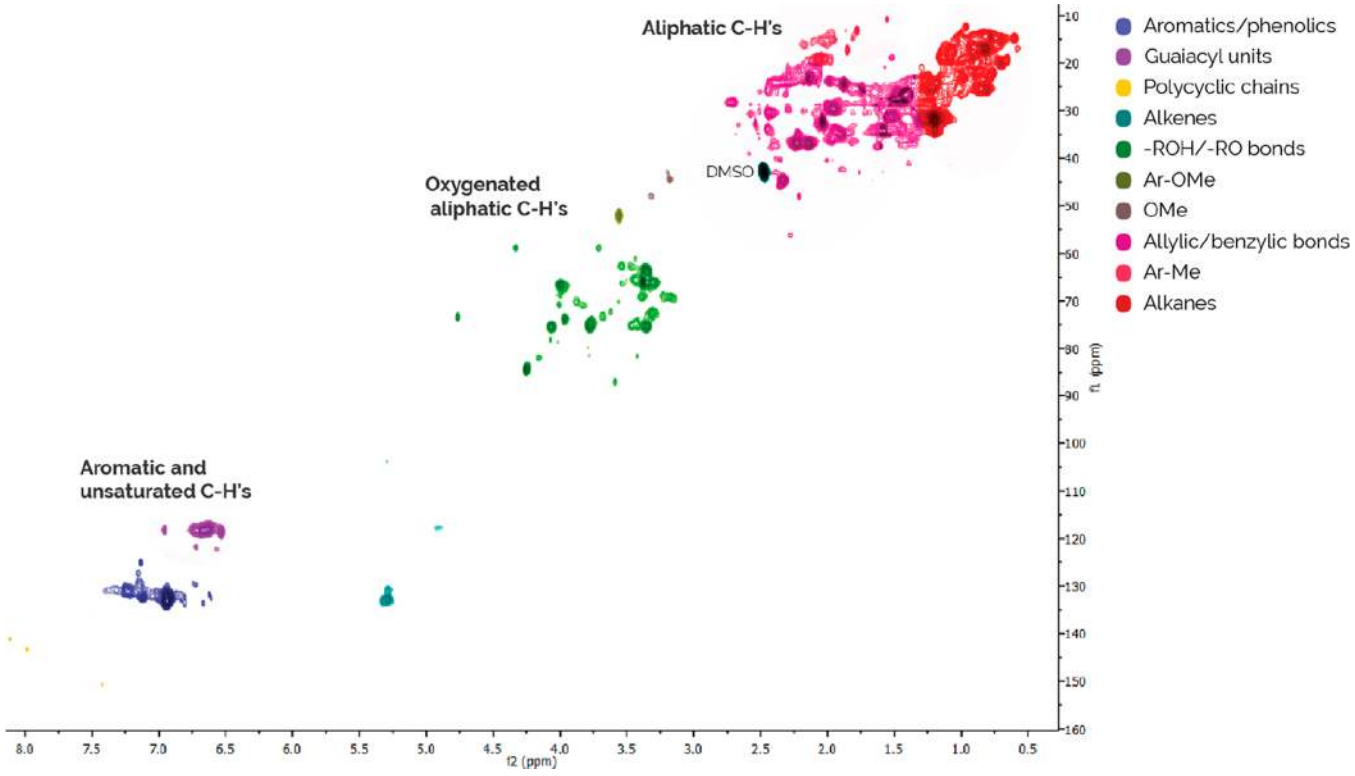

Figure 10. 2D NMR spectra obtained from the sisal residue bio-oil.

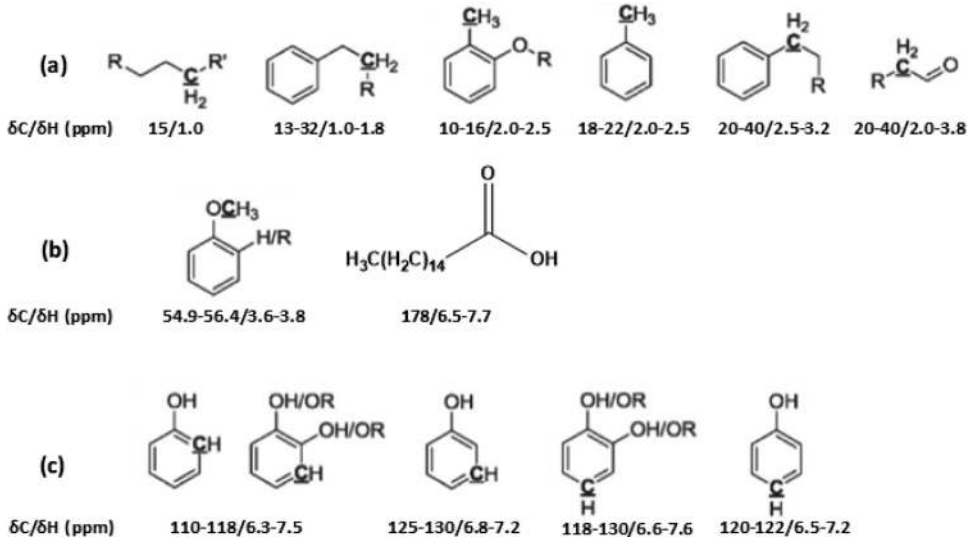

Figure 11. Possible structures of aliphatic (a), oxygenated aliphatic (b) and aromatic components of sisal residue bio-oil (c).

quantitative analysis of each spectral region, for purposes of estimating the distribution of the bonds. The results show a larger area for the region of nonoxygenated aliphatic compounds, which was visually verified in the NMR spectrum. The aromatic region accounted for around 12.3% (i.e., 8% of aromatic and phenolic structures and 4.31% of guaiacyl structures).

All correlations are consistent with the molecular structures identified by GC-qMS, which also confirmed the presence of these types of compounds in the bio-oil taken from the sisal residue.

GC/qMS analysis was performed to identify the monomers in the bio-oil produced by the pyrolysis of the sisal residue. It is possible to observe from Figure 12 the predominance of phenolic compounds in the bio-oil, in addition to a diversity of compounds, such as carboxylic acids, ketones, alcohols, hydrocarbons, amines, and ethers. A total of 39 compounds were identified, as shown in Table 9. The produced bio-oil contains a complex mixture of organic compounds having in the main carbon chain from 2 to 24 carbon atoms. The phenols are the predominant monomers in the bio-oil, representing 21.06% in area based on the detectable fraction, and 4-butyl-phenol (peak 21) is the major compound among the other species. The predominance of phenolic compounds in the bio-oil is in agreement with the results obtained in the FTIR analysis (Figure 8). The use of these compounds in

DOI: 10.1021/acs.energyfuels.8b01718
Energy Fuels 2018, 32, 9478−9492

Table 8. Distribution of the NMR HSQC Areas for the Bio-Oil

group	% area
alkanes	31.68
aromatic-methyl	5.61
allylic/benzylic chains	36.99
ome (methoxy)	1.36
aromatic-ome	0.67
ROH + RO structures	8.30
alkenes	2.49
guaiacyl units	4.31
aromatic/phenolic structures	8.50
polycyclic aromatics	0.08

future industrial applications is the focus of numerous scientific studies,[62] and such achievements still represent a challenge for researchers when they come from bio-oil.

3.3.2. Biochar Characteristics and Properties. Biochar may exhibit some characteristics as high porosity, significant pore structure, and higher volatile matter released, having a great potential for use in many applications: cheap absorbent, carbon coating, solid fuel, and soil amendment.[23,24] It can also be used as a carbon source for producing different carbon materials such as activated carbon, carbon nanotubes, and carbon fibers.[23] Biochar characterization was performed to evaluate its potential for future applications.

The pores present in the biochar were formed during the thermochemical process of fast pyrolysis, which, due to the high temperatures applied, provided a size reduction of the biomass particles and the creation of larger pores.[63] The micrograph of sisal biochar presented a highly anisotropic porous structure (Figure 13), characterized by parallel channels running in the axial direction due to the raw material and the organization of cellulose microfibrils in the lignocellulosic biomass structure.[64] The pore sizes vary from 16.67 to 42.00 μm, corresponding to mesopores (2−50 μm). The porosity of the biochar can be attributed to the elimination of volatile organic compounds from the vegetal residue during pyrolysis. The thermal degradation of the biomass caused the release of volatile organic compounds, which can directly influence the properties of the solid product generated.[65]

The FTIR spectrum of the biochar from the sisal residue is shown in Figure 14. Comparing the spectra of the initial biomass (Figure 5) with the biochar, significant changes in the shape and intensity of the bands can be observed. The band at 3387 cm^{-1} is observed in both of the spectra and refers to the stretching vibrations of the O−H bonds of water.[36,66] Bands around 2925, 1624, and 1450 cm^{-1} are related to methylene and methyl C−H bonds, C═C aromatic compounds, and C−C aromatic ring deformations, respectively.[66]

The biochar obtained from the pyrolysis is a fine, amorphous powder. The reduction of particle size can be associated to three factors: (i) the biomass granulometry required in the process; (ii) tensile strength decrease during the reaction (fast pyrolysis), generating a material with lower resistance to abrasion, and (iii) higher heating rates, resulting in smaller biomass particle sizes and greater generation of volatile products, resulting in the formation of a fine solid material.

Analyzing Table 10 it is possible to observe that the biochar presented a typical and specific surface area of carbonized lignocellulosic biomass; however, the specific surface area of the biochar is much lower than the one observed for commercial activated carbon, which is of approximately 835 $m^2\ g^{-1}$.[67]

4. CONCLUSION

The sisal residue pyrolysis in a fluidized bed reactor was performed in nine different operational conditions in order to identify the largest absolute bio-oil production. The experimental planning technique showed that the effects of the temperature and the flow rate of biomass on the bio-oil yield were significant, with R^2 adj equal to 0.91, indicating that the mathematical model generated by the experimental data can perform predictions with low variability in relation to the mean. Although the highest bio-oil yield occurred under intermediary operating conditions, a relatively high yield could also be achieved under higher conditions. Accordingly, both conditions can be used: if the focus is to maximize the bio-oil yield, the first condition should be preferred, and if the focus is producing noncondensable gases to reduce the costs, the second case should be preferred, if there is, of course, an overall economic viability for the process. Therefore, the choice of the best operational conditions should be made according to one's convenience and possible restrictions, either its yield or economic aspects.

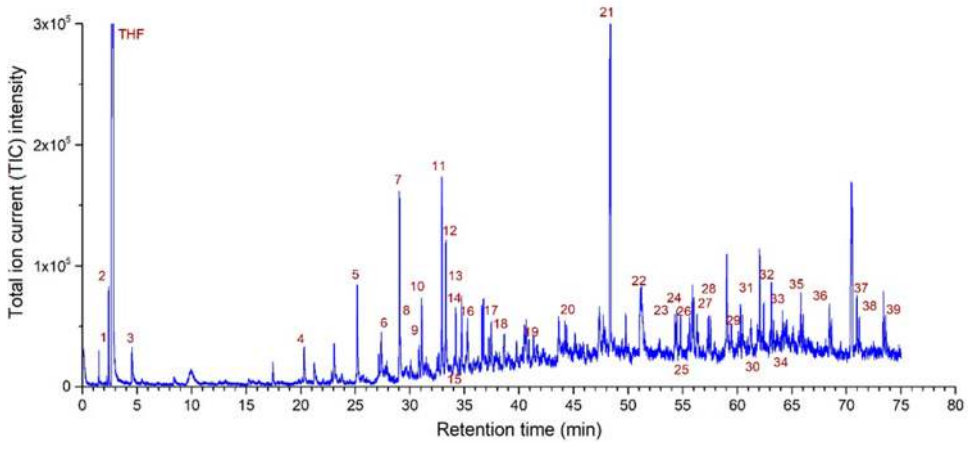

Figure 12. Chromatogram of the bio-oil components of sisal residue by CG/qMS.

DOI: 10.1021/acs.energyfuels.8b01718
Energy Fuels 2018, 32, 9478−9492

Table 9. Compounds Identified by CG/qMS[a]

peak	retention time (min)	compound	molecular formula	peak area (%)
1	2.41	1-methoxybutane	$C_5H_{12}O$	0.88
2	2.84	1-pentanol	$C_5H_{12}O$	1.33
3	4.53	acetic acid	$C_2H_4O_2$	0.44
4	20.33	dihydrofuran-2(3*H*)-one	$C_4H_6O_2$	0.29
5	25.19	phenol	C_6H_6O	1.33
6	27.39	2-methylphenol	C_7H_8O	0.44
7	29.05	4-methylphenol	C_7H_8O	2.65
8	29.14	3-methylpheno	C_7H_8O	0.44
9	30.85	2-ethylphenol	$C_8H_{10}O$	0.59
10	31.09	2,4-dimethylphenol	C8H10O	1.33
11	32.95	4-ethylphenol	C8H10O	2.80
12	33.30	dianhydromannitol	$C_6H_{10}O$	2.50
13	34.21	2-ethyl-4-methylphenol	$C_9H_{12}O$	1.03
14	24.53	3,4-diethylphenol	$C_{10}H_{14}O$	0.29
15	34.75	2,3,6-trimethylphenol	$C_9H_{12}O$	1.03
16	36.61	4-propylphenol	$C_9H_{12}O$	0.88
17	37.48	2,5-diethylphenol	$C_{10}H_{14}O$	0.59
18	38.19	2,5-dimethylbenzenamine	$C_8H_{11}N$	0.15
19	41.62	5-methyl-1*H*-indole	C_9H_9N	0.15
20	45.13	2-methyl-1,3-benzenediol	$C_7H_8O_2$	0.15
21	48.37	4-butyl-phenol	$C_{10}H_{14}O$	8.69
22	51.12	3-(*p*-hydroxyphenyl)-1-propanol	$C_9H_{12}O_2$	1.77
23	54.28	eicosane	$C_{20}H_{42}$	0.29
24	54.81	2-heptadecanone	$C_{17}H_{34}O$	0.59
25	55.64	oxacycloheptadec-8-en-2-one	$C_{16}H_{28}O_2$	1.77
26	56.01	*Z*-1,6-tridecadiene	$C_{13}H_{24}$	0.88
27	57.36	dodecane	$C_{12}H_{26}$	0.59
28	57.53	1-octadecene	$C_{18}H_{36}$	0.29
29	59.05	*n*-hexadecanoic acid	$C_{16}H_{32}O_2$	1.62
30	61.93	bicyclo[3.3.2]decan-9-one	$C_{10}H_{16}O$	0.44
31	62.06	8-dodecenol	$C_{12}H_{24}O$	1.62
32	62.44	1,9-tetradecadiene	$C_{14}H_{26}$	0.88
33	64.52	1-methyldecahydronaphthalene	$C_{11}H_{20}$	0.59
34	64.59	*cis*-1,2-cyclohexanedicarbonitrile	$C_8H_{10}N$	0.29
35	66.04	1-tetradecene	$C_{14}H_{28}$	0.88
36	68.45	hexadecane	$C_{16}H_{34}$	1.03
37	71.17	heptafluorobutanoic acid	$C_4HF_7O_2$	0.74
38	73.40	2-methyl eicosane	$C_{21}H_{44}$	1.18
39	73.60	cyclotetracosane	$C_{24}H_{48}$	0.74

[a]THF (tetrahydrofuran): TR = 2.80; peak area = 93.21%.

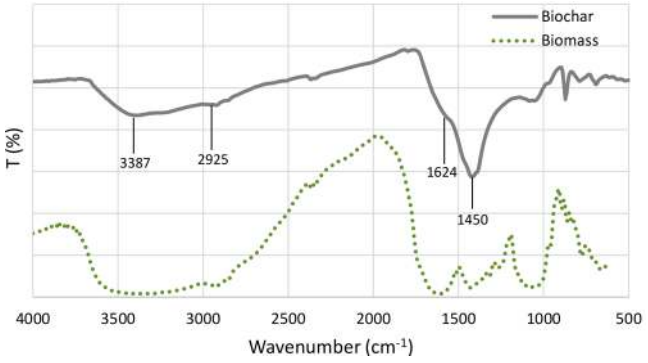

Figure 14. FTIR spectra of pyrolysis carbon.

Table 10. Textural Properties of the Biochar

specific surface area ($m^2\ g^{-1}$)	micropore/volume ($cm^3\ g^{-1}$)	mesopore/volume ($cm^3\ g^{-1}$)
14.2463	0.002257	0.021469

The characterization of the sisal residue showed that the cellulose and hemicellulose fractions are relatively lower in relation to other biomasses; however, the lignin remains within the same range as fixed in the literature. Reduced levels of cellulose and hemicellulose generally produce heavier bio-oil and, in the case of the sisal residue, also involved proteins and extractives, which comprise the bulk of this biomass. Besides that, the high ash and low water content contributed to the high viscosity observed in the bio-oil.

The produced bio-oil consists of a complex heterogeneous mixture of aromatics, fatty acids, alkenes, and alkanes. Several monomers could be identified by GC-MS, especially phenolics and acids, while the 2D NMR analysis revealed a high concentration of aliphatic bonds, followed by aromatics and oxygenated aliphatics. In addition, one of the three major units involved in lignin biosynthesis (i.e., guaiacyl) could be identified, and the presence of only one related CH signal suggests a high degree of substitution for this type of structure. In addition, guaiacyl generated only one signal, of three possible, suggesting that G units have a high degree of substitution. The molecular weight distribution was shown to be similar to other pyrolytic materials, consisting of a mixture low molecular fragments (i.e., 63% of the produced molecules were in the range of monomers-tetramers) and oligomers. The final average molecular weight was 414.2 g/mol, signifying the high level of cracking that occurred during the pyrolysis process.

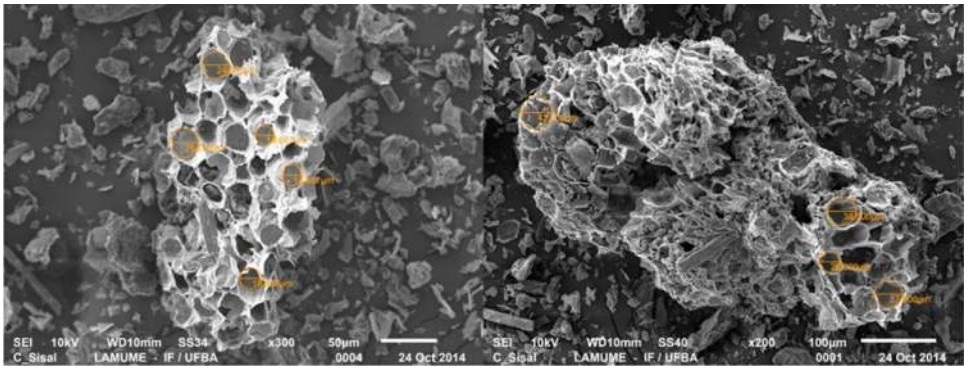

Figure 13. SEM image of the charcol.

DOI: 10.1021/acs.energyfuels.8b01718
Energy Fuels 2018, 32, 9478−9492

H_2, CO, CO_2, CH_4 and other gases have been identified and quantified in the noncondensable gas stream. Their levels predict that they can be used as fuel and as a source of synthesis gas; however, the separation of these gases from the nitrogen (major gas) and from each other depends on the evolution of the separation technology. A H_2/CO ratio of 2.16 could be achieved, which is a suitable value for the further production of methanol and liquid biofuels.

The biochar of the sisal residue presented a specific surface area is much lower than the one observed for commercial activated carbon; however, it can be increased by physic or chemical activation producing an activated carbon due to be used as a precursor in the synthesis of low cost high performance porous catalysts supports. Additionally, high ash content in biochar indicated its potential usage as a biofertilizer as well as an absorbent. On the other hand, a lower carbon content in biochar suggests that it is not recommended as solid fuel in furnaces.

Our research shows the potential of the bio-oil produced from the fast pyrolysis of sisal residue to be used as a source of biobased fuels and phenolics. The further development of an optimized pyrolysis process able to maximize the bio-oil yields, together with the application of downstream separation steps, are key challenges that must be addressed in order to achieve the necessary feasibility. Noncondensable gas and biochar should be commercially exploited in parallel with bio-oil. Although its applications are at different stages of development, biochar is the product of greatest potential for immediate exploitation can be used in the domestic sector, the industrial sector, and as an input for the activated charcoal production. However, the most suitable product for further application is bio-oil due to the higher added value of its chemicals.

Finally, the possibility of adding value to a lignocellulosic waste can bring significant benefits to the rural areas currently involved with the exploitation of sisal, as well as contribute to the establishment of sustainable solutions and renewable sources of platform chemicals and energy.

AUTHOR INFORMATION

Corresponding Author

*E-mail: cap@ufba.br.

ORCID

Luis Gabriel G. Pereira: 0000-0002-1055-0300

Carlos Augusto M. Pires: 0000-0003-4231-6495

Notes

The authors declare no competing financial interest.

ACKNOWLEDGMENTS

This work was supported by the Bahia State Foundation for Research Support-FAPESB (Project DTE: 0061/2011).

REFERENCES

(1) Broeren, M. L. M.; Dellaert, S. N. C.; Cok, B.; Patel, M. K.; Worrell, E.; Shen, L. Life cycle assessment of sisal fiber e Exploring how local practices can influence environmental performance. *J. Cleaner Prod.* **2017**, *149*, 818−827.

(2) FAOSTAT. *Food and Agricultural Commodities Production/Countries by Commodity*; http://www.fao.org/faostat/en/#home, Accessed date: July 09 2017.

(3) Oliveira, I. F. *Semi-Arid Bahia - The Contradictory Dynamics of Development*, 1st ed.; São Paulo: Baraúna, 2015 (in Portuguese).

(4) Araújo, A. E.; Sousa, M. F.; Silva, O. R. R. F.; Cartaxo, W. V.; Coutinho, W. M. *Sisal Production Chain in the Brazilian Northeast.* Embrapa Algodão, Sistema de Produção, 5 ISSN 1678-8710, 2014; https://www.spo.cnptia.embrapa.br/conteudo?p_p_id=conteudoportlet_WAR_sistemasdeproducaolf6_1ga1ceportlet&p_p_lifecycle=0&p_p_state=normal&p_p_mode=view&p_p_col_id=column-1&p_p_col_count=1&p_r_p_ 6293187_sistemaProducaoId=3716&p_r_p_996514994_topicoId=3284, Accessed date: March 20, 2018.

(5) *AGEITEC- Agência Embrapa de Informação Tecnológica*, 2009; Disponível em: http://www.agencia.cnptia.embrapa.br/gestor/milho/arvore/CONT000fya0krse02wx5ok0pvo4k3mp7ztkf.html, Accessed date: August 22 2016.

(6) Fraga, A. *Modernization of the Sisal Production Chain Will Open New Markets*. http://revistagloborural.globo.com/Noticias/Agricultura/noticia/2014/02/modernizacao-da-cadeia-produtiva-do-sisal-vai-abrir-novos-mercados.html, Accessed date: November 5 2017.

(7) Karvonen, J.; Kunttu, J.; Suominen, T.; Kangas, J.; Leskinen, P.; Judl, J. Integrating fast pyrolysis reactor with combined heat and power plant improves environmental and energy efficiency in bio-oil production. *J. Cleaner Prod.* **2018**, *183*, 143−152.

(8) Venderbosch, R. H.; Prins, W. Fast pyrolysis technology development. *Biofuels, Bioprod. Biorefin.* **2010**, *4*, 178−208.

(9) Oasmaa, A.; Solantausta, Y.; Arpiainen, V.; Kuoppala, E.; Sipila, K. Fast Pyrolysis Bio-Oils from Wood and Agricultural Residues. *Energy Fuels* **2010**, *24*, 1380−1388.

(10) Bridgwater, A. V. Review of fast pyrolysis of biomass and product upgrading. *Biomass Bioenergy* **2012**, *38*, 68−98.

(11) Pereira, L. G. G.; Pires, C. A. M. The effect of temperature on the flow profile of the bio-oil produced from the fast pyrolysis of sisal residue. *Energy Fuels* **2017**, *31*, 2871−2878.

(12) Mesa, J. M.; Rocha, J. D.; Olivares, E.; Barboza, L. A.; Brossard, L. E.; Brossard Junior, L. E. Pirólise rápida em leito fluidizado: uma opção para transformar biomassa em energia limpa. *Ver. Anal.* **2003**, *4*, 32−36.

(13) Bridgwater, A. V. Biomass fast pyrolysis. *Review Paper* **2004**, *8*, 21−49.

(14) Wang, Q.; Li, X.; Wang, K.; Zhu, Y.; Wang, S. *Commercialization and Challenges for the Next Generation of Biofuels: Biomass Fast Pyrolysis*; IEEE, 2010; 978-1-4244-4813-5/10.

(15) Hao, S.; Chen, K.; Cao, L.; Zhu, X.; Luo, G.; Zhang, S.; Chen, J. Separation of high-purity syringol and acetosyringone from rice straw-derived bio-oil by combining the basification-acidification process and column chromatography. *Electrophoresis* **2016**, *37* (19), 2522−2530.

(16) Lozano, F. J.; Lozano, R. Assessing the potential sustainability benefits of agricultural residues: Biomass conversion to syngas for energy generation or to chemicals production. *J. Cleaner Prod.* **2018**, *172*, 4162−4169.

(17) Vithanage, A. E.; Chowdhury, E.; Alejo, L. D.; Pomeroy, P. C.; Desisto, W. J.; Frederick, B. G.; Gramlich, W. M. Renewably sourced phenolic resins from lignin bio-oil. *J. Appl. Polym. Sci.* **2017**, *134* (19), 1−10.

(18) Choi, H. S.; Choi, Y. S.; Park, H. C. The influence of fast pyrolysis condition on biocrude-oil yield and homogeneity. *Korean J. Chem. Eng.* **2010**, *27* (4), 1164−1169.

(19) Bridgwater, A. V.; Meier, D.; Radlein, D. An overview of fast pyrolysis of biomass. *Org. Geochem.* **1999**, *30*, 1479−1493.

(20) Bridgwater, A. V. Renewable fuels and chemicals by thermal processing of biomass. *Chem. Eng. J.* **2003**, *91* (2), 87−102.

(21) Butler, E.; Devlin, G.; Meier, D.; Mcdonnell, K. A review of recent laboratory research and commercial developments in fast pyrolysis and upgrading. *Renewable Sustainable Energy Rev.* **2011**, *15* (8), 4171−4186.

(22) Bello, M. M.; Raman, A. A. A.; Purushothaman, M. Applications of fluidized bed reactors in wastewater treatment − A review of the major design and operational parameters. *J. Cleaner Prod.* **2017**, *141*, 1492−1514.

DOI: 10.1021/acs.energyfuels.8b01718
Energy Fuels 2018, 32, 9478−9492

(23) Sellin, N.; Krohl, D. R.; Marangoni, C.; Souza, O. Oxidative fast pyrolysis of banana leaves in fluidized bed reactor. *Renewable Energy* **2016**, *96*, 56−64.
(24) Pradhan, D.; Singh, R. K.; Bendu, H.; Mund, R. Pyrolysis of Mahua seed (Madhuca indica) − Production of biofuel and its characterization. *Energy Convers. Manage.* **2016**, *108*, 529−538.
(25) Carrier, M.; Joubert, J.; Danje, S.; Hugo, T.; Görgens, J.; Knoetze, J. Impact of the lignocellulosic material on fast pyrolysis yields and product quality. *Bioresour. Technol.* **2013**, *150*, 129−138.
(26) Asadullah, M.; Rasid, N. S. A.; Kadir, S. A. S. A.; Azdarpour, A. Production and detailed characterization of bio-oil from fast pyrolysis of palm kernel shell. *Biomass Bioenergy* **2013**, *59*, 316−324.
(27) Arazo, R. O.; Genuino, D. A. D.; de Luna, M. D. G.; Capareda, S. C. Bio-oil production from dry sewage sludge by fast pyrolysis in an electrically-heated fluidized bed reactor. *Sustain. Environ. Res.* **2017**, *27*, 7−14.
(28) Carvalho, W. S.; Santana Júnior, J. A.; de Oliveira, T. J. P.; Ataíde, C. H. Fast pyrolysis of sweet sorghum bagasse in a fluidized bed reactor: Product characterization and comparison with vapors generated in analytical pyrolysis. *Energy* **2017**, *131*, 186−197.
(29) Bridgwater, A. V.; Peacocke, G. V. C. Fast pyrolysis processes for biomass. *Renewable Sustainable Energy Rev.* **2000**, *4*, 1−73.
(30) Silva, D. J.; Queiroz, A. C. *Food Analysis: Chemical and Biological Methods*, 3rd ed.; Viçosa, Imprensa Universitária, 2002; p 235 (in Portuguese).
(31) Antal, M. J., Jr.; Allen, S. G.; Dai, X.; Shimizu, B.; Tam, M. S.; Grønli, M. Attainment of the Theoretical Yield of Carbon from Biomass. *Ind. Eng. Chem. Res.* **2000**, *39*, 4024−4031.
(32) Foo, K. Y.; Hameed, B. H. Preparation, characterization and evaluation of adsorptive properties of orange peel based activated carbon via microwave induced K_2CO_3 activation. *Bioresour. Technol.* **2012**, *104*, 679−686.
(33) Carvalho, G. G. P.; Pires, A. J. V. Organização dos tecidos de plantas forrageiras e suas implicações para os ruminantes. *Zootecnia* **2008**, *57* (1), 13−28.
(34) Martin, A. R.; Martins, M. A.; Mattoso, L. H.; Silva, O. R. R. F. Caracterização química e estrutural de fibra de sisal da variedade Agave Sisalana, Polímeros. *Polim.: Cienc. Tecnol.* **2009**, *19* (1), 40−46.
(35) Raveendran, K.; Ganesh, A.; Khilar, K. C. Pyrolysis characteristics of biomass and biomass components. *Fuel* **1996**, *75* (8), 987−998.
(36) de Lima, A. C. A.; Nascimento, R. F.; de Sousa, F. F.; Filho, J. M.; Oliveira, A. C. Modified coconut shell fibers: A green and economical sorbent for the removal of anions from aqueous solutions. *Chem. Eng. J.* **2012**, *185-186*, 274−284.
(37) Ramos, P. H.; Guerreiro, M. C.; Resende, E. C.; Gonçalves, M. Production and characterization of activated carbon prepared from PVA defect coffee. *Quim. Nova* **2009**, *32*, 1139.
(38) Rosa, M. F.; Chiou, B. S.; Medeiros, E. S.; Wood, D. F.; Mattoso, T. G. W.; Williams, L. H. C.; Orts, J.; Imam, S. H. Biodegradable composites based on starch/EVOH/glycerol blends and coconut fibers. *Bioresour. Technol.* **2009**, *100*, 5196−5202.
(39) Airoldi, C.; Vieira, A. P.; Santana, S. A. A.; Bezerra, C. W. B.; Silva, H. A. S.; Chaves, J. A. P.; da Silva Filho, E. C. S.; de Melo, J. C. P. Kinetics and thermodynmics of textile dye adsonption from aqueous solutions using babassu coconut mesocarp. *J. Hazard. Mater.* **2009**, *166*, 1272−1278.
(40) Palkar, R. R.; Shilapuram, V. Detailed parametric design methodology for hydrodynamics of liquid−solid circulating fluidized bed using design of experiments. *Particuology* **2017**, *31*, 59−68.
(41) Behainne, J. J. R.; Martinez, J. D. Performance analysis of an air-blown pilot fluidized bed gasifier for rice husk. *Energy Sustainable Dev.* **2014**, *18*, 75−82.
(42) Yusup, S.; Khan, Z.; Ahmad, M. M.; Rashidi, N. A. Optimization of hydrogen production in in-situ catalytic adsorption (ICA) steam gasification based on Response Surface Methodology. *Biomass Bioenergy* **2014**, *60*, 98−107.
(43) Pereira, L. G. G.; Pires, C. A. M. Bio-oil viscosity of sisal residue: process and temperature influence. *Energy Fuels* **2018**, *32*, 5115−5124.
(44) Zhang, H.; Hu, J.; Zheng, J.; Xiao, R. Fast pyrolysis of cellulosic ethanol solid residues with high ash and lignin contents in a fluidized bed. *J. Anal. Appl. Pyrolysis* **2017**, *128*, 217−223.
(45) Jendoubi, N.; Broust, F.; Commandre, J. M.; Mauviel, G.; Sardin, M.; Lédé, J. Inorganics distribution in bio oils and char produced by biomass fast pyrolysis: The key role of aerosols. *J. Anal. Appl. Pyrolysis* **2011**, *92*, 59−67.
(46) Nayan, N. K.; Kumar, S.; Singh, R. K. Characterization of the liquid product obtained by pyrolysis of karanja seed. *Bioresour. Technol.* **2012**, *124*, 186−189.
(47) Nayan, N. K.; Kumar, S.; Singh, R. K. Production of the liquid fuel by thermal pyrolysis of neem seed. *Fuel* **2013**, *103*, 437−443.
(48) Mesa-Pérez, J. M.; Rocha, J. D.; Barbosa Cortez, L. A.; Penedo-Medina, M.; Luengo, C.; Cascarosa, E. Fast oxidative pyrolysis of sugar cane straw in a fluidized bed reactor. *Appl. Therm. Eng.* **2013**, *56* (1−2), 167−175.
(49) Singh, V. K.; Soni, A. B.; Kumar, S.; Singh, R. K. Pyrolysis of sal seed to liquid product. *Bioresour. Technol.* **2014**, *151*, 432−435.
(50) Shadangi, K. P.; Mohanty, K. Comparison of yield and fuel properties of thermal and catalytic Mahua seed pyrolytic oil. *Fuel* **2014**, *117*, 372−380.
(51) Gouda, N.; Singh, R. K.; Patel, R. K.; Panda, A. K. Fast pyrolysis of Kaner (Thevetia peruviana) Seed to Fuel and Chemicals. *Int. J. Appl. Anal. Chem.* **2015**, *1* (1), 7−20.
(52) Moralı, U.; Yavuzel, N.; Şensöz, S. Pyrolysis of hornbeam (Carpinus betulus L.) sawdust: Characterization of bio-oil and bio-char. *Bioresour. Technol.* **2016**, *221*, 682−685.
(53) Kurzina, I. A.; Reshetnikov, S. I.; Karakchieva, N. I.; Kurina, L. N. Direct synthesis of dimethyl ether from synthesis gas: Experimental study and mathematical modeling. *Chem. Eng. J.* **2017**, *329*, 135−141.
(54) Duanguppama, K.; Suwapaet, N.; Pattiya, A. Fast pyrolysis of contaminated sawdust in a circulating fluidised bed reactor. *J. Anal. Appl. Pyrolysis* **2016**, *118*, 63−74.
(55) Speight, J. G. *Petroleum Chemistry and Refining*; Taylor & Francis, Western Research Institute, Laramie, Wyoming, USA, 1998.
(56) Li, L.; Yuan, X.; Zeng, G.; Huang, D.; Huang, H.; Tong, J.; You, Q.; Zhang, J.; Zhou, M. The formation of bio-oil from sludge by deoxy-liquefaction in supercritical ethanol. *Bioresour. Technol.* **2010**, *101*, 2860−2866.
(57) Kim, S.-J.; Jung, S.-H.; Kim, J.-S. Fast pyrolysis of palm kernel shells: Influence of operation parameters on the bio-oil yield and the yield of phenol and phenolic compounds. *Bioresour. Technol.* **2010**, *101*, 9294−9300.
(58) Michailof, C. M.; Kalogiannis, K. G.; Sfetsas, T.; Patiaka, D. T.; Lappas, A. A. Advanced analytical techniques for bio-oil characterization. *Wires. Energy. Environ.* **2016**, *5* (6), 614−639.
(59) Mattsson, C.; Andersson, S.-I.; Belkheiri, T.; Åmand, L.-E.; Olausson, L.; Vamling, L.; Theliander, H. Using 2D NMR to characterize the structure of the low and high molecular weight fractions of bio-oil obtained from LignoBoost kraft lignin depolymerized in subcritical water. *Biomass Bioenergy* **2016**, *95*, 364−377.
(60) del Rio, J. C.; Rencoret, J.; Marques, G.; Li, J.; Gellerstedt, G.; Jiménez-Barbero, J. J.; Martínez, A. T.; Gutiérrez, A. J. Structural Characterization of the Lignin from Jute (Corchorus capsularis) Fibers. *J. Agric. Food Chem.* **2009**, *57*, 10271−10281.
(61) Fortin, M.; Beromi, M. M.; Lai, A.; Tarves, P. C.; Mullen, C. A.; Boateng, A. A.; West, N. M. West, Structural Analysis of Pyrolytic Lignins Isolated from Switchgrass Fast-Pyrolysis Oil, Energy Fuels. *Energy Fuels* **2015**, *29*, 8017−8026.
(62) Zhu, X.; Zhu, Y.; Zhang, Y.; Li, F.; Xin, S. Potentiometric and semi-empirical quantum chemical studies on liquid−liquid micro-extraction of 4-tert-butylphenol with trioctyl phosphate clusters. *Arabian J. Chem.* **2017**, *10*, S3774−S3780.
(63) Brewer, C. E.; Schmidt-Rohr, K.; Satrio, J. A.; Brown, R. C. Characterization of biochar from fast pyrolysis and gasification systems. *Environ. Prog. Sustainable Energy* **2009**, *28* (3), 386−396.

DOI: 10.1021/acs.energyfuels.8b01718
Energy Fuels 2018, 32, 9478−9492

(64) Scala, F.; Chirone, R.; Salatino, P. Salatino. Combustion and attrition of biomass chars in a fluidized bed. *Energy Fuels* **2006**, *20* (1), 91−102.
(65) Ma, S.; Lu, J.; Gao. Study of the low temperature pyrolysis of PVC. *Energy Fuels* **2002**, *16* (2), 338−342.
(66) Bandosz, T. J.; Ania, C. O. *Surface Chemistry of Activated Carbons and Its Characterization*; Elsevier, Interface Science and Technology, 2006, *7*; p 159.
(67) Lota, G.; Centeno, T. A.; Frackowiak, E.; Stoeckli, F. Improvement of the structural and chemical properties of a commercial activated carbon for its application in electrochemical capacitors. *Electrochim. Acta* **2008**, *53* (5), 2210−2216.

DOI: 10.1021/acs.energyfuels.8b01718
Energy Fuels 2018, 32, 9478−9492